Traveling Waves of Excitation in Neural Field Models: Equivalence of Rate Descriptions and Integrate-and-Fire Dynamics

Daniel Cremers
cremers@uni-mannheim.de
Department of Mathematics and Computer Science, University of Mannheim, 68131 Mannheim, Germany

Andreas V. M. Herz
a.herz@biologie.hu-berlin.de
Innovationskolleg Theoretische Biologie, Humboldt-Universität zu Berlin, 10115 Berlin, Germany

Field models provide an elegant mathematical framework to analyze large-scale patterns of neural activity. On the microscopic level, these models are usually based on either a firing-rate picture or integrate-and-fire dynamics. This article shows that in spite of the large conceptual differences between the two types of dynamics, both generate closely related plane-wave solutions. Furthermore, for a large group of models, estimates about the network connectivity derived from the speed of these plane waves only marginally depend on the assumed class of microscopic dynamics. We derive quantitative results about this phenomenon and discuss consequences for the interpretation of experimental data.

1 Introduction

Traveling waves of synchronized neural excitation occur in various brain regions and play an important role both during development and for information processing in the adult. Such waves have been observed in various systems, including the retina (Meister, Wong, Denis, & Shatz, 1991), olfactory bulb (Gelperin, 1999), visual cortex (Bringuier, Chavane, Glaeser, & Fregnac, 1999), and motor cortex (Georgopoulos, Kettner, & Schwartz, 1988). In vitro, excitation waves have been successfully induced to probe single-neuron dynamics as well as large-scale connectivity patterns (Traub, Jefferys, & Miles, 1993; Wadman & Gutnick, 1993; Golomb & Amitai, 1997).

The omnipresence of traveling waves in neural tissues is reflected by a wealth of models, ranging from detailed biophysical approaches (Traub et al., 1993; Destexhe, Bal, McCormick, & Sejnowski, 1996; Golomb & Amitai, 1997; Rinzel, Terman, Wang, & Ermentrout, 1998) to highly simplified mathematical formulations (Beurle, 1956; von Seelen, 1968; Wilson & Cowan,

1973; Amari, 1977; Ermentrout & Cowan, 1979; Idiart & Abbott, 1993; Ben-Yishai, Hansel, & Sompolinsky, 1997; Horn & Opher, 1997; Ermentrout, 1998; Kistler, Seitz, & van Hemmen, 1998; Bressloff, 1999; Golomb & Ermentrout, 1999; Bressloff, 2000; Kistler, 2000; Golomb & Ermentrout, 2001). Models of the latter type have to sacrifice biological realism to a certain extent, but they often admit a quantitative analysis of the relation between the accessible macroscopic wave phenomena and otherwise hidden aspects of the neural dynamics and connectivity patterns. In some mathematical models, for example, the speed of the emergent traveling wave can be expressed in closed form in terms of the parameters describing single-neuron behavior and network circuitry (Idiart & Abbott, 1993; Ben-Yishai et al., 1997; Horn & Opher, 1997; Ermentrout, 1998; Kistler et al., 1998; Bressloff, 1999, 2000; Golomb & Ermentrout, 1999, 2001; Kistler, 2000). Given one of these models, results from large-scale neurophysiological measurements may be directly interpreted in terms of microscopic neural parameters.

Most of the mathematical models describing spatiotemporal activity patterns are formulated as field models in continuous space. Within these models, two broad classes can be distinguished: firing-rate models and models with spiking neurons. The former, more traditional, field models are based on a locally averaged neuronal firing rate. The latter, more recent, class of field models incorporates the existence of action potentials. Here, the local dynamics involve the generation of action potentials, for example, through an integrate-and-fire mechanism.

A traveling wave in a firing-rate model typically corresponds to the spread of a region with a high firing rate (Wilson & Cowan, 1973; Amari, 1977; Idiart & Abbott, 1993). As depicted in Figure 1, this is in sharp contrast to the simplest traveling wave in a system with spiking neurons, where both before and directly behind the wave front, activity is low so that the resulting neural activation pattern is highly localized in space and time. Depending on the refractory period, synaptic timescales, and heterogeneity of intrinsic and coupling properties, the activation pattern in a model with spiking neurons may also exhibit complicated spatiotemporal structures, including multiple reexcitations behind the wave front. Numerical simulations show, however, that these phenomena have almost no effect on the speed of the wave front (Ermentrout, 1998).

Independent of the precise structure of traveling waves in firing-rate models and systems with spiking neurons, there is no doubt that the two types of wave correspond to entirely different dynamical scenarios. Are these two scenarios nevertheless related to each other on a mathematical level, even if they describe two highly distinct biological situations? If so, can results obtained within one framework be applied to phenomena observed in the other setting?

This article addresses these questions and shows that surprisingly there is a close connection between the two model classes. In particular, it is demonstrated that for a large group of commonly used systems, there exists
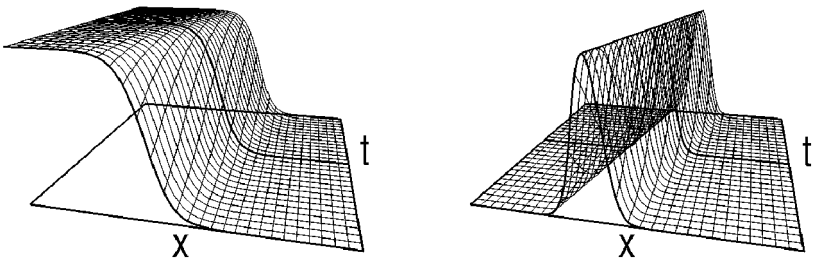
Figure 1: Schematic space-time plots of the simplest traveling wave in a one-dimensional firing-rate model (left) and an integrate-and-fire model (right). The spatial activity at two different times is highlighted by thick lines. In the firing-rate model, the wave front connects a region with a low firing rate with a region with a high firing rate. In the integrate-and-fire model, on the other hand, activity is low both before and directly behind the wave front. Reexcitation may lead to more complicated activity profiles but has almost no effect on the speed of the wave front. This justifies the study of simplified integrate-and-fire models with a single narrow activity peak as depicted on the right side.

a one-to-one mapping between the two classes. This mapping involves a nontrivial geometric transformation of the neural connectivity pattern. As a consequence, biological interpretations of experimental measurements in terms of the underlying neural circuitry may depend strongly on the assumed class of model dynamics. We derive quantitative results about this effect, discuss implications for data analysis, and close with some remarks on extensions and limitations of this approach.

2 Field Models Based on Mean-Firing-Rate Descriptions

In traditional field models such as those proposed by Wilson and Cowan (1973) or Amari (1977), neural activity is treated as a phenomenological variable $u(x, t)$ that represents the local short-time averaged membrane potential. In this continuum approximation, the time evolution of neural activity is described by a partial differential equation, for example, the frequently used prototype

$$\tau \frac{\partial u(x, t)}{\partial t} = -u(x, t) + \int_{-\infty}^{t} dt'\, \alpha(t - t')$$

$$\cdot \int dy\, J(x - y) g\left[u\left(y, t' - \frac{|x - y|}{c} \right) \right]. \qquad (2.1)$$

It describes the dynamics of one homogeneous population of neurons. The parameter τ denotes an effective membrane time constant, and $J(z)$ models the distance dependence of synaptic coupling strengths, often in the

form of a Mexican hat type of interaction with strong short-range excitation surrounded by weak inhibition. A prominent example for the functional form of such distance-dependent coupling strengths is the difference of two gaussians. The function $g(u)$ characterizes the nonlinear dependence of the firing rate on the mean local membrane potential. Such activation functions are usually modeled by sigmoid functions, that is, monotone increasing and s-shaped functions that approach zero for $u \to -\infty$ and saturate for $u \to +\infty$. Note that within this class of model, firing rates and mean membrane potentials are treated on the same footing, simply related by the static nonlinearity g.

The kernel α captures the dynamical effects of signal delays and (post)-synaptic integration processes. For example, $\alpha(s) = \delta(s - \tau_{\text{axon}})$ describes a discrete uniform delay, and

$$\alpha(s) = \tau_{\text{psp}}^{-1} e^{-s/\tau_{\text{psp}}} \Theta(s) \tag{2.2}$$

or

$$\alpha(s) = s \tau_{\text{psp}}^{-2} e^{-s/\tau_{\text{psp}}} \Theta(s) \tag{2.3}$$

mimic two commonly used time courses of postsynaptic potentials. Distance-dependent axonal propagation delays are taken care of by the term $|x - y|/c$ in the argument of u in equation 2.1, where c denotes the signal propagation velocity. In the mathematical analysis, we will neglect the effects of finite c and set $1/c = 0$ for simplicity. From a neurobiological point of view, this is justified if characteristic velocities of the large-scale activity patterns are small compared to the axonal signal velocity. All our results do, however, generalize to finite propagation speed.

In what follows, we assume that, on average, excitatory synaptic interactions are stronger than inhibitory interactions. This means that the temporal and spatial kernels can be taken to be normalized to plus one,

$$\int_0^\infty ds\, \alpha(s) = 1 \tag{2.4}$$

and

$$\int_{-\infty}^\infty dz\, J(z) = 1. \tag{2.5}$$

Temporal integration of equation 2.1 results in the integral equation

$$u(x, t) = \int_{-\infty}^t dt'\, \epsilon(t - t') \int dy\, J(x - y) g[u(y, t')] \tag{2.6}$$

with

$$\epsilon(s) = \tau^{-1} \int_0^s ds' \, e^{-\frac{s-s'}{\tau}} \alpha(s'). \tag{2.7}$$

As a consequence of equation 2.4, the kernel ϵ is also normalized,

$$\int_0^\infty ds \, \epsilon(s) = 1. \tag{2.8}$$

As will become apparent in the following sections, the integral formulation, equation 2.6, is most suitable for discussing wave phenomena.

3 Wave Fronts in One-Dimensional Firing-Rate Models

Because of the normalizations 2.5 and 2.8, all homogeneous and stationary solutions $u(x, t) = u$ of equation 2.6 satisfy a simple fixed-point equation,

$$u = g(u). \tag{3.1}$$

Depending on the shape of g, equation 3.1 allows a single or multiple solutions. Of particular interest are sigmoid functions with three solutions $u_r < u_u < u_e$. Here, u_r corresponds to the stable rest state of a neuron (low firing rate), u_e, to the stable excited state (high firing rate), and u_u, to the intermediate unstable equilibrium. In this case of a bistable network, a traveling wave joining the rest state u_r and the excited state u_e can be triggered for appropriate initial conditions. For example, if $\lim_{x \to -\infty} u(x, 0) = u_e$ and $\lim_{x \to \infty} u(x, 0) = u_r$, a wave of excitation may propagate in the positive x-direction through the system.

If g vanishes for u less than a fixed threshold $\vartheta > 0$,

$$g(u) = 0 \qquad \text{for} \qquad u < \vartheta, \tag{3.2}$$

the rest state is given by $u_r = 0$, and finding traveling wave fronts of equation 2.6 simplifies significantly, as shown by Idiart and Abbott (1993). Consider again a wave propagating in the positive x-direction that reaches the point x_0 at time t_0, that is, $u(x_0, t_0) = \vartheta$. Since the wave is approaching from the left, $g[u(y, t')] = 0$ for all $y > x_0$ as long as $t' < t_0$. Thus, although in general the activity $u(y, t')$ itself is nonzero in front of the wave, due to the condition 3.2, this has no effect on the dynamics for $u < \vartheta$. (See Figure 2.) Evaluated at $x = x_0$ and $t = t_0$, equation 2.6 therefore reads

$$\vartheta = u(x_0, t_0) = \int_{-\infty}^{t_0} dt' \, \epsilon(t_0 - t') \int_{-\infty}^{x_0} dy \, J(x_0 - y) g[u(y, t')]. \tag{3.3}$$
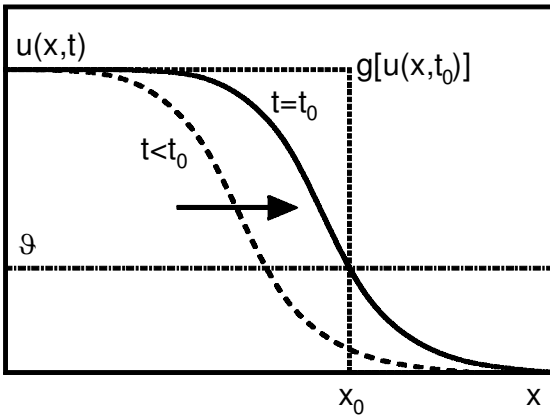
Figure 2: Schematic plot of a wave front in a firing-rate model. The wave is traveling in the positive x-direction, as indicated by the arrow. The profile of neural excitation $u(x, t)$ is shown at two instances: at $t = t_0$ by a solid line, and at some earlier time $t < t_0$ by a dashed line. In addition, the profile of $g[u(x, t)]$ is depicted for $t = t_0$ by a dotted line. Notice that although $u(x, t_0)$ is nonzero for all x, $g[u(x, t_0)]$ vanishes for $x > x_0$ because a threshold nonlinearity with $g(u) = 0$ for $u < \vartheta$ was chosen.

If one inserts the traveling-wave ansatz,

$$u(x, t) = \tilde{u}(t - x/v), \tag{3.4}$$

into equation 3.3, influences of the structure of J and the shape of g on the propagation velocity v may readily be analyzed (Idiart & Abbott, 1993).

4 Field Models Based on Integrate-and-Fire Neurons

The models described above are based on a firing-rate description of neural activity and neglect the existence of action potentials. More recently, a different class of field models has been introduced that explicitly incorporates the spiking nature of neural activity (Ermentrout, 1998; Kistler et al., 1998; Bressloff, 1999, 2000; Golomb & Ermentrout, 1999, 2001; Kistler, 2000).

On the single-cell level, the most salient features of spiking neurons are captured by integrate-and-fire models. Here, each neuron integrates synaptic inputs and generates a uniform action potential whenever the membrane potential crosses a fixed threshold from below. Simulations with networks of regularly spaced integrate-and-fire neurons reveal a large variety of macroscopic activity patterns such as plane waves, rotating spirals and expanding rings (see, for example, Fohlmeister, Gerstner, Ritz, & van Hemmen, 1995; Ermentrout, 1998; Horn & Opher, 1997; Kistler et al., 1998).

The length of the refractory period influences the profile of traveling waves in systems with spiking neurons. Depending on the model parameters, shapes range from narrow soliton-like excitations, where each neuron fires only once, to complex activity profiles due to multiple reexcitations behind the wave front. However, extensive numerical investigations provide strong evidence that the speed of a traveling wave front is largely independent of subsequent spike activity (Ermentrout, 1998). This result justifies the study of models without reexcitation, such as one-dimensional systems of the type

$$\tau \frac{\partial V(x, t)}{\partial t} = -V(x, t) + \int_{-\infty}^{\infty} dy\, C(x - y)\, \tilde{\alpha}[t - t^{\star}(y)] \tag{4.1}$$

where $V(x, t)$ describes the local membrane potential, $C(z)$ represents synaptic coupling strengths, and $\tilde{\alpha}$ captures transmission phenomena as in section 2. The time $t^{\star}(y)$ denotes the firing time of a neuron at location y, determined by the conditions $V(y, t^{\star}) = \vartheta$ and $\partial V(y, t)/\partial t > 0$ for $t = t^{\star}$ (Ermentrout, 1998).

With the definition

$$\rho(s) = \tau^{-1} \int_{0}^{s} ds'\, e^{-\frac{s-s'}{\tau}}\, \tilde{\alpha}(s'), \tag{4.2}$$

integration of equation 4.1 results in the integral equation

$$V(x, t) = \int_{-\infty}^{t} dt'\, \rho(t - t') \int_{-\infty}^{\infty} dy\, C(x - y)\delta[V(y, t') - \vartheta]$$
$$\cdot \left| \frac{\partial V(y, t')}{\partial t'} \right| \Theta \left[\frac{\partial V(y, t')}{\partial t'} \right], \tag{4.3}$$

where $\Theta(\cdot)$ denotes the Heaviside step function. A dynamical description that is closely related to equation 4.3 was obtained by Kistler (2000), who also provided a mathematical proof that the dynamics of a spatially discretized network approaches the dynamics of a neural field model if the characteristic length scale of neural interactions is much larger than the grid size. In this limit, the membrane potential V at location x and time t becomes

$$V(x, t) = \int_{-\infty}^{t} dt'\, \rho(t - t') \int_{-\infty}^{\infty} dy\, C(x - y)S(y, t')$$
$$+ \int_{-\infty}^{t} dt'\, \eta(t - t')S(x, t'), \tag{4.4}$$

where spike activity at location y and time t' is now denoted by $S(y, t')$, and ρ and C model the temporal and spatial aspects of signal transmission and

integration similar to equation 2.1. Refractoriness following local spike activity results from hyperpolarization, whose time course is described by $\eta(s)$.

Spike activity is triggered whenever the local field crosses a threshold ϑ from below,

$$S(x, t) = \delta[V(x, t) - \vartheta] \left| \frac{\partial V(x, t)}{\partial t} \right| \Theta \left[\frac{\partial V(x, t)}{\partial t} \right]. \tag{4.5}$$

According to the derivation given by Kistler, the variables $V(x, t)$ and $S(x, t)$ can be interpreted as interpolated versions of the corresponding variables $V(x_i, t)$ and $S(x_i, t)$ of the original spatially discretized network, where neuron i, with $1 \le i \le N$, is located at site x_i. From a neurophysiological point of view, this implies that $V(x, t)$ and $S(x, t)$ mimic different components of the local field potential recorded at location x, with $V(x, t)$ representing averaged postsynaptic potentials and $S(x, t)$ describing the effects of spike activity.

Equation 4.5 implies that elementary spike activity is described by a δ-function whose size, when integrated over time, is normalized to unity (Ermentrout, 1998; Bressloff, 1999, 2000; Golomb & Ermentrout, 1999; Kistler, 2000). This normalization reflects the unitary character of action potentials. In an alternative approach by Kistler et al. (1998), the factor $|\frac{\partial V(x,t)}{\partial t}|$ is replaced by $|\frac{\partial V(x,t)}{\partial x}|$ so that spike activity is normalized when integrated in the spatial domain. However, as pointed out by Bressloff (1999), and acknowledged in Kistler (2000), only the first description, equation 4.5 is biophysically justified.

Focusing on the wave front of a traveling wave, we may neglect the possible occurrence of reexcitations and set the second term on the right-hand side of equation 4.4 to zero without loss of generality. Inserting equation 4.5 into 4.4 then yields 4.3 as desired.

5 Mapping the Firing-Rate Model onto the Integrate-and-Fire Model ___

Although at first glance, equation 4.3 is somewhat reminiscent of 2.6, the two classes of neural field models are quite different from a conceptual point of view. The first assumes that the response properties of a neuron are fully described by its firing rate. As a consequence, the local field $u(x, t)$ in equation 2.1 represents a postsynaptic membrane potential that has been averaged in both space and time. Within the integrate-and-fire field model, in contrast, no temporal average is carried out; the variable $S(x, t)$ in equation 4.5 represents spike activity whose time evolution is given by an integrate-and-fire mechanism. Despite these differences, both types of model show similar macroscopic patterns such as traveling waves of excitation, but the details of these waves differ significantly, as illustrated in Figure 1.
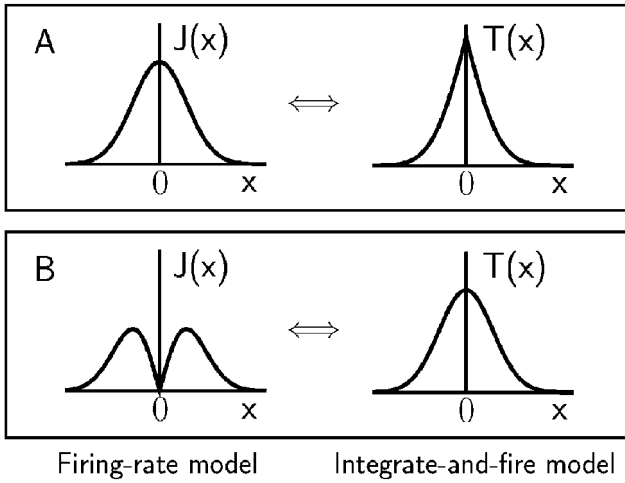
Figure 3: Corresponding synaptic connectivities in firing-rate and integrate-and-fire models. Each of the two panels, *A* and *B*, shows one example of a *J* coupling (firing-rate model, left side) and a *T* coupling (integrate-and-fire model, right side). In the upper panel, gaussian couplings are assumed for the firing-rate model and lead to a strongly peaked coupling distribution for the integrate-and-fire model. In the lower panel, gaussian couplings are assumed for the integrate-and-fire model and imply a coupling distribution for the firing-rate model that is peaked away from zero.

What is the relation between the two approaches? To investigate this questions, we will now map the dynamics of the firing-rate model onto the dynamics of the integrate-and-fire model.

We focus on the case of a propagating wave front as described in section 3 and denote its propagation velocity by v. Furthermore, we assume symmetric J couplings, $J(z) = J(-z)$, that are continuous and integrable.

We introduce auxiliary couplings $T(z)$ by

$$T(z) := \begin{cases} v^{-1} \int_{-\infty}^{z} dz'\, J(z'), & z < 0, \\ v^{-1} \int_{z}^{\infty} dz'\, J(z'), & z \geq 0. \end{cases} \tag{5.1}$$

(See Figure 3.) Due to the assumptions for $J(z)$, these new couplings are also symmetric, $T(z) = T(-z)$, and continuous at $z = 0$ with

$$T(0) = \frac{1}{2v}. \tag{5.2}$$

In terms of the T couplings, the original J couplings are given by

$$J(z) = \begin{cases} +v\frac{d}{dz}T(z), & z < 0, \\ -v\frac{d}{dz}T(z), & z \geq 0. \end{cases} \tag{5.3}$$

By definition, the T couplings vanish for large positive and negative argument. Note that apart from the special case of exponential couplings, $J(z) \propto \exp(-|z|/\sigma)$, the couplings $J(z)$ and $T(z)$ do not have the same shape. Using integration by parts, we obtain for the second integral in equation 3.3,

$$\int_{-\infty}^{x_0} dy\, J(x_0 - y)g[u(y, t')]$$

$$= v \int_{-\infty}^{x_0} dy \left(\frac{\partial}{\partial y}T(x_0 - y) \right) g[u(y, t')]$$

$$= v\, T(0)\, g[u(x_0, t')] - v \int_{-\infty}^{x_0} dy\, T(x_0 - y)h[u(y, t')]\frac{\partial u(y, t')}{\partial y} \tag{5.4}$$

with

$$h(u) := \frac{dg(u)}{du}. \tag{5.5}$$

Because $T(0)$ is finite and $g[u(x_0, t')]$ vanishes for all $t' < t_0$, inserting equation 5.4 into equation 3.3 results in

$$\vartheta = u(x_0, t_0)$$

$$= v \int_{-\infty}^{t_0} dt'\, \epsilon(t_0 - t') \int_{-\infty}^{x_0} dy\, T(x_0 - y)h[u(y, t')]\left|\frac{\partial u(y, t')}{\partial y}\right|$$

$$= \int_{-\infty}^{t_0} dt'\, \epsilon(t_0 - t') \int_{-\infty}^{x_0} dy\, T(x_0 - y)h[u(y, t')]\left|\frac{\partial u(y, t')}{\partial t'}\right|, \tag{5.6}$$

where we have employed the identity $v \cdot |\frac{\partial u(y,t')}{\partial y}| = |\frac{\partial u(y,t')}{\partial t'}|$ and the fact that the wave is traveling in the positive x-direction so that $\partial u/\partial y \leq 0$.

Due to the particular definition of the T couplings (see equation 5.1), equation 5.6 also holds for waves traveling in the negative x-direction. In this case, $\partial u/\partial y \geq 0$ and $J(x_0 - y) = -\frac{d}{dy}T(x_0 - y)$ in the relevant region of space $(y > x_0)$.

The above calculations hold for any kind of threshold nonlinearity (see equation 3.2). For the commonly considered case where the nonlinearity $g(u)$ is a step function (see, for example, Amari, 1977),

$$g(u) = \Theta(u - \vartheta), \tag{5.7}$$

the function h becomes a δ-function,

$$h(u) = \delta(u - \vartheta), \tag{5.8}$$

and equation 5.6 reduces to

$$\begin{aligned}
\vartheta &= u(x_0, t_0) \\
&= \int_{-\infty}^{t_0} dt'\, \epsilon(t_0 - t') \int_{-\infty}^{x_0} dy\, T(x_0 - y) \delta[u(y, t') - \vartheta] \left| \frac{\partial u(y, t')}{\partial t'} \right| \\
&= \int_{-\infty}^{t_0} dt'\, \epsilon(t_0 - t') \int_{-\infty}^{x_0} dy\, T(x_0 - y) \delta[u(y, t') - \vartheta] \\
&\quad \cdot \left| \frac{\partial u(y, t')}{\partial t'} \right| \Theta \left[\frac{\partial u(y, t')}{\partial t'} \right].
\end{aligned} \tag{5.9}$$

In the last step, we used the fact that $\partial u / \partial t > 0$ at threshold crossing. The comparison of equation 5.9 with equation 4.3, evaluated for $x = x_0$ and $t = t_0$, reveals that equation 5.9 is identical with the threshold condition for a wave front in the integrate-and-fire field model if we identify $u(x, t) = V(x, t), \epsilon(\tau) = \rho(\tau)$, and $C(z) = T(z)$.

This finding implies that the wave front in a one-dimensional field model with step nonlinearity is equivalent to the wave front in a field model with integrate-and-fire neurons. Note, however, that the spatial couplings in both models are not the same but related via the transformation 5.1.

More generally, even firing-rate models with smooth sigmoid nonlinearities $g(u)$ can be mapped onto integrate-and-fire models, as shown by equation 5.6. In that case, the shape of an action potential in the associated integrate-and-fire model is not any longer given by a δ-function as for step nonlinearities but rather by the expression

$$S(x, t) = \frac{dg[u(x, t)]}{du} \left| \frac{\partial u(x, t)}{\partial t} \right|. \tag{5.10}$$

Depending on the shape of g, different action-potential shapes may thus be modeled.

6 From Macroscopic Wave Phenomena to Microscopic Dynamics

Let us investigate the interpretation of an electrophysiological experiment of the type performed by Traub et al. (1993), Wadman and Gutnick (1993), or Golomb and Amitai (1997) in which a wave velocity v has been measured in some neural substrate. What are the differences between the inferred system parameters depending on whether we base our calculations on a rate model, as in Idiart and Abbott (1993) or an integrate-and-fire mechanism

as in Ermentrout (1998)? This question is an extreme case of a situation often encountered in a model-based analysis of neurophysiological data: How do assumptions about the underlying dynamics influence the system parameters derived from experimental measurements?

In the present case, we can answer this question analytically and gain further insight into the scope and limitations of deriving network characteristics from the properties of waves of neural excitation. To do so, we assume some functional form for the true synaptic couplings $C(z)$. For concreteness, we take the couplings to be gaussians with standard deviation σ. Within the firing-rate model, we therefore set $J(z) = C(z)$ and denote σ by σ_J. Within the integrate-and-fire model, we have to derive $J(z)$ through equation 5.3 from gaussian couplings $T(z)$ with $\sigma = \sigma_T$. The T couplings thus have the same shape as $C(z)$ but are normalized according to equation 5.2 so that in both scenarios, the J couplings satisfy the normalization 2.5 to guarantee an unbiased comparison. Keeping all other parameters fixed, we then derive analytical expressions for σ_J and σ_T, compare their values, and may thus judge how strongly the inferred network parameters depend on the assumptions about the single-cell dynamics.

We present three different examples of this approach. In the first example, we investigate the general model, equation 2.1, with finite signal propagation speed $c < \infty$. Inserting the traveling wave ansatz 3.4 into equation 3.3 and integrating by parts with respect to t', we can extend the approach of Idiart and Abbott (1993), who focused on the specific case $\alpha(s) = \delta(s)$. We obtain for step nonlinearities, $g(u) = \Theta(u - \vartheta)$, the following implicit equation for v,

$$\vartheta = \int_{-\infty}^{0} dz\, J(z) \int_{0}^{-\gamma z} \epsilon(s)\, ds, \tag{6.1}$$

with

$$\gamma = v^{-1} - c^{-1}, \tag{6.2}$$

where the wave is, as before, traveling in the positive x-direction. Assuming that the shape $\alpha(s)$ of a postsynaptic potential is exponentially decaying (see equation 2.2), we get

$$\epsilon(t) = \frac{1}{\tau_{psp} - \tau} (e^{-t/\tau_{psp}} - e^{-t/\tau})\Theta(t), \tag{6.3}$$

and equation 6.1 becomes

$$\vartheta = \int_{-\infty}^{0} dz\, J(z) \left[1 - \frac{1}{\tau_{psp} - \tau} (\tau_{psp} e^{-\gamma |z|/\tau_{psp}} - \tau e^{-\gamma |z|/\tau}) \right]. \tag{6.4}$$

To simplify the mathematics, we consider couplings whose spatial range is small compared to the distance the wave travels in the time interval $\tilde{\tau} = \min\{\tau, \tau_{psp}\}$ relevant for the microscopic dynamics. In other words, we focus on the case where

$$\int_{-\infty}^{0} dz\, |z|^n J(z) \ll (v\tilde{\tau})^n \quad \forall n \in \mathbf{N}. \tag{6.5}$$

In this regime, we can neglect higher-order terms in the expansion of the exponential functions in equation 6.4 and obtain

$$\vartheta \approx \frac{\gamma^2}{\tau\,\tau_{psp}} \int_{-\infty}^{0} dz\, J(z) z^2. \tag{6.6}$$

To answer the question posed in the beginning of this section, we now consider on the one hand gaussian J couplings and arrive at $\int_{-\infty}^{0} dz\, J(z) z^2 = \sigma_J^2/2$. If, on the other hand, we use gaussian T couplings with proper normalization (see equation 5.2), we obtain $\int_{-\infty}^{0} dz\, J(z) z^2 = \sigma_T^2$. Independent of values for τ, τ_{psp}, c, and v, the estimates for σ_J and σ_T are therefore always related by

$$\sigma_J = \sqrt{2}\sigma_T. \tag{6.7}$$

We now turn to a second example and assume instantaneous interactions without any signal delays, $\alpha(s) = \delta(s)$, so that $\epsilon(s) = \tau^{-1} e^{-s/\tau}$. For gaussian J couplings, we can solve equation 6.1 and obtain

$$\vartheta = \frac{1}{2} - \exp\left(\frac{\gamma^2 \sigma_J^2}{2\tau^2}\right) \mathrm{erf}\left(\frac{-\gamma\,\sigma_J}{\tau}\right), \tag{6.8}$$

where $\mathrm{erf}(x)$ denotes the error function. If, on the other hand, we take T couplings with gaussian shape, we get

$$\vartheta = \frac{1}{2} - \exp\left(\frac{\gamma^2 \sigma_T^2}{2\tau^2}\right) \sqrt{\frac{\pi}{2}} \frac{\gamma\,\sigma_T}{\tau} \mathrm{erf}\left(\frac{-\gamma\,\sigma_T}{\tau}\right). \tag{6.9}$$

Equating the right-hand sides of equations 6.8 and 6.9 for $\gamma\,\sigma \ll \tau$, we obtain

$$\sigma_J = \frac{\pi}{2}\sigma_T. \tag{6.10}$$

Finally, if instead of gaussian couplings, we use block-shaped couplings, $J(z) = 1/(2a_J)$ for $-a_J \leq z \leq a_J$ and zero elsewhere, a calculation similar to equations 6.8 through 6.10 leads to

$$\sigma_J = 2\sigma_T. \tag{6.11}$$

Thus, in these three cases investigated, the width of the same type of synaptic coupling inferred from the measured wave velocity differs by a factor 1.4 to 2 between the firing-rate and integrate-and-fire picture. Furthermore, we obtain $\sigma_J > \sigma_T$ in all three cases. For gaussian couplings C, Figure 3 offers a heuristic explanation of this result: the right-hand side of equation 6.1 depends on the higher-order moments of $J(z)$. For gaussian T couplings (lower right in the figure) with given standard deviation σ_T, the higher-order moments of the derived J couplings (lower left in the figure) are smaller than those of gaussian J couplings (upper left) with the same standard deviation, $\sigma_J = \sigma_T$. To compensate for this difference, we have to choose $\sigma_J > \sigma_T$ as verified by the analytical calculation.

7 Discussion

As shown in this article, wave fronts of traveling waves in firing-rate models and models with integrate-and-fire dynamics are intimately related on a formal level. Taking into account that these descriptions are extreme and opposite caricatures of the true neural dynamics, the differences in the inferred model parameters are surprisingly small and suggest that more elaborate biophysical models might show intermediate results. We may thus conclude that macroscopic wave phenomena can be used reliably to estimate the characteristics of neural dynamics and network architecture that are not directly observable. However, it should be noted that our calculations are based on simple homogeneous single-layer models. Neural tissues with multiple layers, more complicated feedback structures, or additional slow dynamical components might support traveling waves of a rather different nature, as also suggested by results of Rinzel et al. (1998) and Golomb and Ermentrout (1999, 2001). The emergent properties of such neural systems might depend sensitively on the biophysical details of the underlying dynamics.

Our studies have been restricted to integrate-and-fire models that do not exhibit reexcitation. This approach is justified by the observation of Ermentrout (1998) that the speed of a traveling wave front is largely independent of subsequent spiking activity. More elaborate modeling frameworks could also be used to describe nonvanishing asynchronous activity ahead and behind the traveling wave front and to include heterogeneity of neural and synaptic properties. We believe that these extensions offer interesting topics for further research but that they will not change the overall picture about the relation of wave phenomena in firing-rate and integrate-and-fire models. In addition, traveling wave solutions in both types of model are likely to share the same stability properties, but we have not been able to prove this analytically. However, even if the stability of two corresponding solutions differed under certain circumstances, our analysis would still be helpful in that it allows finding unstable waves in one modeling framework by searching for all stable solutions in the

other framework, which, from a numerical point of view, is a much simpler task.

The equivalence of firing-rate and integrate-and-fire models also holds for plane waves in two- and higher-dimensional systems. For concreteness, let us assume that the wave in a three-dimensional firing-rate model is propagating in the x-direction so that $u(x, y, z, t)$ depends on only x and t. We may then reduce the original system to an effective one-dimensional system by defining effective J_{eff}-couplings through $J_{\text{eff}}(x) = \int_{-\infty}^{\infty} dy \int_{-\infty}^{\infty} dz\, J(x, y, z)$ and compute the corresponding T_{eff}-couplings as in equation 5.1. We can therefore describe the original wave within either a one-dimensional firing-rate or a one-dimensional integrate-and-fire picture. In a further step, we may also wish to know which three-dimensional integrate-and-fire models are compatible with the one-dimensional model. To answer this question, we have to search for couplings $T(x, y, z)$ that satisfy $\int_{-\infty}^{\infty} dy \int_{-\infty}^{\infty} dz\, T(x, y, z) = T_{\text{eff}}(x)$. This problem is underdetermined so that we may set additional constraints on $T(x, y, z)$. For example, we can ask which isotropic and homogeneous couplings $\tilde{T}$, $T(x, y, z) = \tilde{T}(x^2 + y^2 + z^2)$ correspond to a given T_{eff}.

Although successful for plane wave solutions, our approach is not useful for circular or spiral waves. These solutions break the translation symmetry of the underlying network and distinguish one specific location: the origin of the expanding wave. If we nevertheless apply our methods and start from homogeneous couplings in the firing-rate or integrate-and-fire framework, we obtain inhomogeneous couplings in the other framework. Furthermore, the coupling strengths explicitly reflect the location of the origin of the specific wave solution. With these limitations in mind, the current approach may help to unify different concepts of neural field dynamics.

Let us close with a final observation about the relation between firing-rate and integrate-and-fire neural network models. Firing-rate dynamics are usually derived from models with spiking neurons by taking short-time averages. In field models with spatially continuous neural activity, a conceptually different method becomes possible: spatial integration of the dynamical variables, together with spatial differentiation of the synaptic couplings. For traveling waves, no information is lost by this transformation. This shows that under certain circumstances, microscopic dynamical descriptions as different as firing-rate and integrate-and-fire models may exhibit equivalent patterns of large-scale activity.

Acknowledgments

References

Amari, S. I. (1977). Dynamics of pattern formation in lateral-inhibition type neural fields. *Biological Cybernetics, 27*, 77–87.

Ben-Yishai, R., Hansel D., & Sompolinsky H. (1997). Traveling waves and the processing of weakly tuned inputs in a cortical network module. *Journal of Computational Neuroscience, 4*, 57–77.

Beurle, R. L. (1956). Properties of a mass of cells capable of regenerating pulses. *Philosophical Transactions of the Royal Society B, 240*, 55–94.

Bressloff, P. C. (1999). Synaptically generated wave propagation in excitable neural media. *Physical Review Letters, 82*, 2979–2982.

Bressloff, P. C. (2000). Traveling waves and pulses in a one-dimensional network of excitable integrate-and-fire neurons. *Journal of Mathematical Biology, 40*, 169–198.

Bringuier, V., Chavane, F., Glaeser, L., & Fregnac, Y. (1999). Horizontal propagation of visual activity in the synaptic integration field of area 17 neurons. *Science, 283*, 695–699.

Destexhe, A., Bal, T., McCormick, D. A., & Sejnowski, T. J. (1996). Ionic mechanisms underlying synchronized oscillations and propagating waves in a model of ferret thalamic slices. *Journal of Neurophysiology, 76*, 2049–2070.

Ermentrout, G. B. (1998). The analysis of synaptically generated traveling waves. *Journal of Computational Neuroscience, 5*, 191–208.

Ermentrout, B., & Cowan, J. (1979). A mathematical theory of visual hallucination patterns. *Biological Cybernetics, 34*, 137–150.

Fohlmeister, C., Gerstner, W., Ritz, R., & van Hemmen, J. L. (1995). Spontaneous excitations in the visual cortex: Stripes, spirals, rings, and collective bursts. *Neural Computation, 7*, 1046–1055.

Gelperin, A. (1999). Oscillatory dynamics and information processing in olfactory systems. *Journal of Experimental Biology, 202*, 1855–1864.

Georgeopoulos, A. P., Kettner, R. E., & Schwartz, A. B. (1988). Primate motor cortex and free arm movements to visual targets in three-dimensional space. II. Coding of the direction of movement by a neuronal population. *Journal of Neuroscience, 8*, 2928–2937.

Golomb, D., & Amitai, Y. (1997). Propagating neuronal discharges in neocortical slices: Computational and experimental study. *Journal of Neurophysiology, 78*, 1199–1211.

Golomb, D., & Ermentrout, G. B. (1999). Continuous and lurching traveling pulses in neuronal networks with delay and spatially decaying connectivity. *Proc. Natl. Acad. Sci. USA, 96*, 13480–13485.

Golomb, D., & Ermentrout, G. B. (2001). Bistability in pulse propagation in networks of excitatory and inhibitory populations. *Phys. Rev. Lett., 86*, 4179–4182.

Horn, D., & Opher, I. (1997). Solitary waves of integrate-and-fire neural fields. *Neural Computation, 9*, 1677–1690.

Idiart, M. A. P., & Abbott, L. F. (1993). Propagation of exitation in neural network models. *Network, 4*, 285–294.

Kistler, W. M. (2000). Stability properties of solitary waves and periodic wave trains in a two-dimensional network of spiking neurons. *Phys. Rev. E, 62*(6), 8834–8837.

Kistler, W. M., Seitz, R., & van Hemmen, J. L. (1998). Modeling collective excitations in cortical tissue. *Physica D, 114*, 273–295.

Meister, M., Wong, R. O. L., Denis, A. B., & Shatz, C. J. (1991). Synchronous bursts of action potentials in ganglion cells of the developing mammalian retina. *Science, 252*, 939–943.

Rinzel, J., Terman, D., Wang, X.-J., & Ermentrout, B. (1998). Propagating activity patterns in large-scale inhibitory neuronal networks. *Science, 279*, 1351–1355.

Traub, R. D., Jefferys, J. G. R., & Miles, R. (1993). Analysis of propagation of disinhibition-induced after-discharges along the guinea-pig hippocampal slice in vitro. *Journal of Physiology, 472*, 267–287.

von Seelen, W. (1968). Informationsverarbeitung in homogenen Netzen von Neuronenmodellen I. *Kybernetik, 5*, 133–148.

Wadman, W. J., & Gutnick, M. J. (1993). Non-uniform propagation of epileptiform discharge in brain slices of rat neocortex. *Neuroscience, 52*, 255–262.

Wilson, H. R., & Cowan, J. D. (1973). A mathematical theory of the functional dynamics of cortical and thalamic nervous tissue. *Kybernetik, 13*, 55–80.